Leibniz-Institut für Astrophysik Potsdam

Observations of Solar Magnetic Activity

Carsten Denker and Meetu Verma

Abstract. The solar magnetic field drives solar activity on a wide range of spatial and temporal scales and with different morphologies throughout the solar atmosphere, from the photosphere and chromosphere to the transition region and corona. High-resolution observations of the solar magnetic field now provide access to the fundamental scales at which hot plasma and magnetic fields interact. Ground-based solar telescopes with aperture diameters larger than one meter and their advanced instruments have provided many case studies covering all facets of solar activity. This review focuses on high-resolution photospheric and chromospheric observations, linking them to synoptic observations and bridging the gap in spatial and temporal coverage.

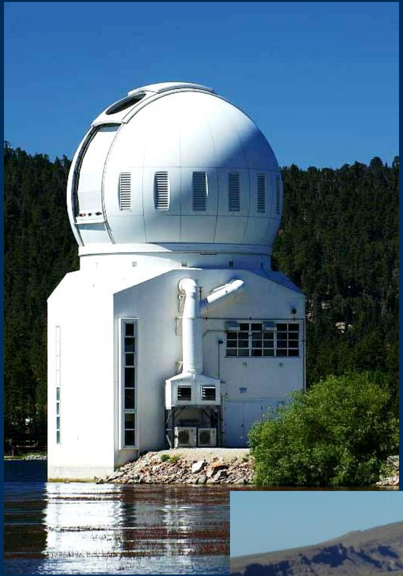

Motivation

- Large-aperture telescopes
  - 1.7-meter Goode Solar Telescope (GST) at Big Bear Solar Observatory (BBSO) in California $\rightarrow$ 2009
  - 1.5-meter GREGOR solar telescope at Observatorio del Teide, Tenerife, Spain $\rightarrow$ 2012
  - 4-meter Daniel K. Inouye Solar Telescope (DKIST) at Haleakala Observatory, Maui, Hawaii $\rightarrow$ 2019
  - 4-meter European Solar Telescope (EST)
- 15 years of high-resolution solar observations (one telescope every 5 years)
- Overview of scientific work with a focus on solar magnetic activity
- Only selected studies will be presented.
- High-resolution observations from other telescopes are missing
  - 1-meter Swedish Solar Telescope (SST)
  - 1-meter balloon-borne SUNRISE telescope
  - 0.7-meter Vacuum Tower Telescope (VTT)
  - 0.5-meter Solar Optical Telescope (SOT) onboard the Hinode mission

Sunspots and Pores

Magnetic Field Oscillations in a Pore

- GREGOR Infrared Spectrograph (GRIS)
  → IFU Fe I λ1564.85 nm line (SIR)
- Localized (<1″) oscillations of 100+ G and longer (600+ s) amplitude (200+ G) variations

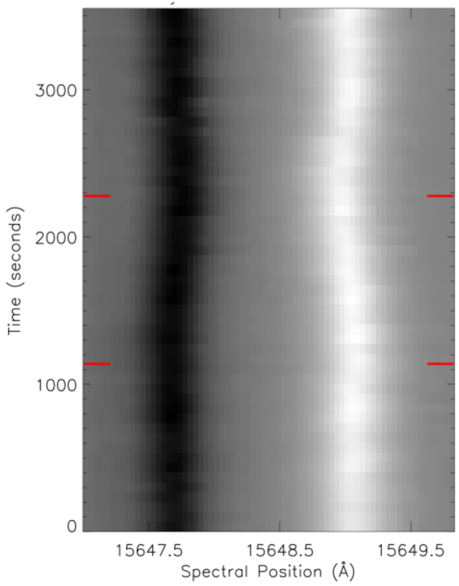

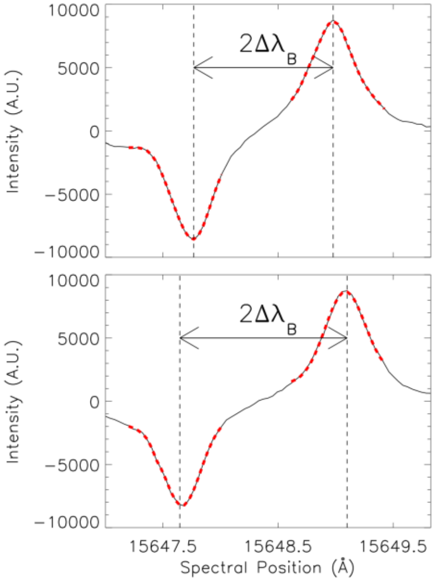

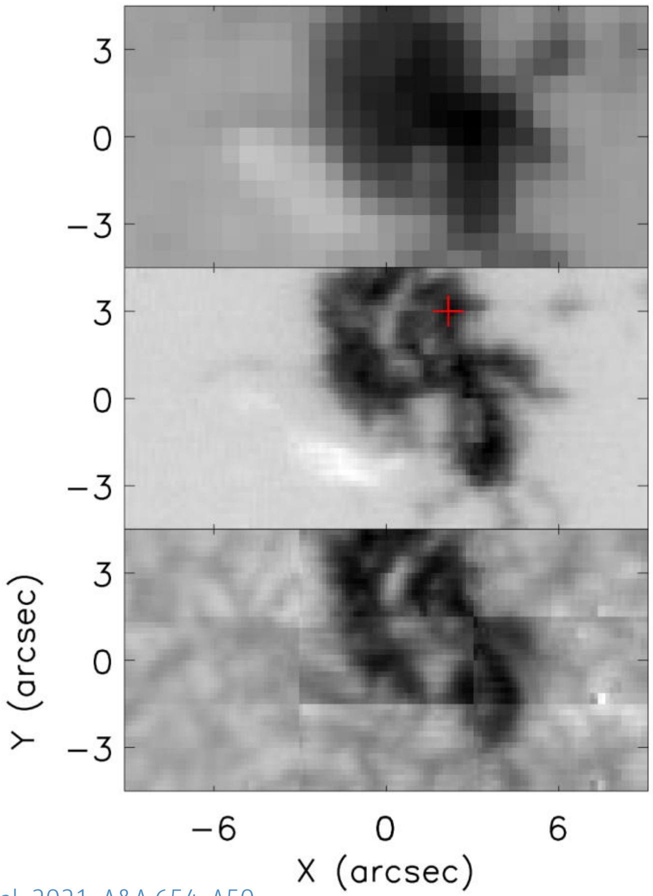

Nelson et al. 2021, A&A 654, A50

GREGOR

Horizontal Flow Fields in and around an Active Region

- Blue Imaging Channel (BIC) at GREGOR → Fraunhofer G-band
- Helioseismic and Magnetic Imager (HMI) → LOS magnetic field
- Local correlation tracking (LCT) and differential affine velocity estimator (DAVE) → horizontal proper motions during emergence and decay of a small active region

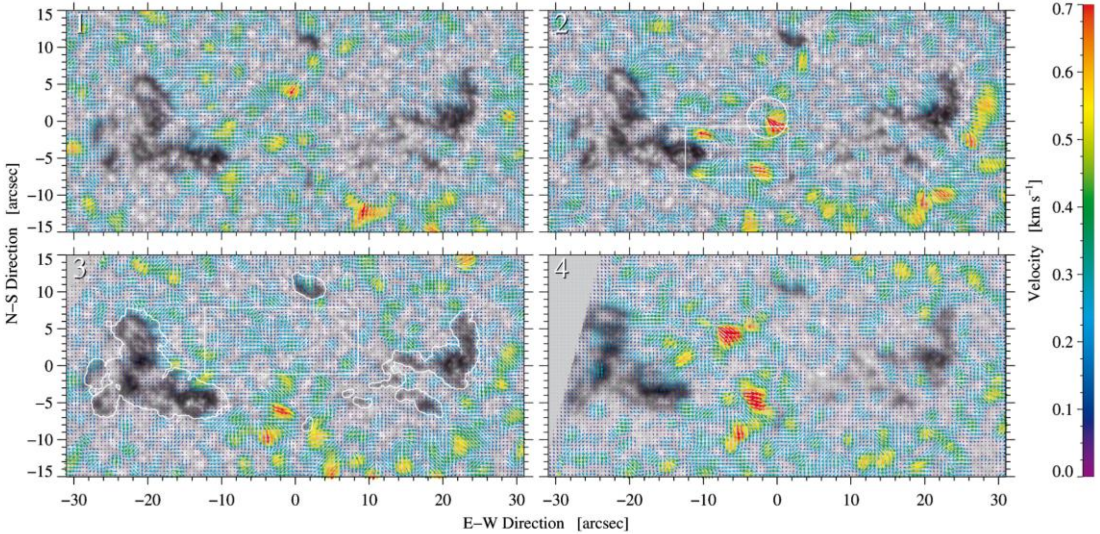

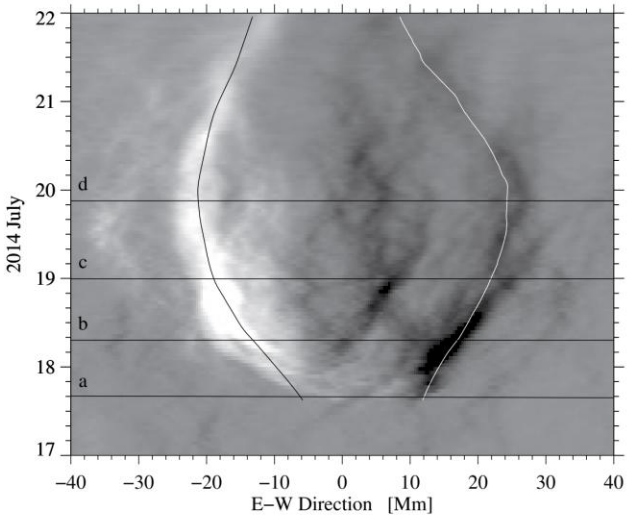

Verma et al. 2016, A&A 596, A3

- Growth rates for photometric area, magnetic area, and magnetic flux are twice as high as the respective decay rates.
- Diverging feature indicates flux emergence and upwelling plasma.

Magnetic Flux Transport in a Decaying Sunspot

- GST Near Infra- Red Imaging Spectro-polarimeter (NIRIS) → LOS magnetic field
- GST Visible Imaging Spectrometer (VIS) → Hα imaging spectroscopy
- GST Broadband Filter Imager (BFI) → TiO λ706 nm
- Area and total magnetic flux → exponential decrease during decay
- Moving magnetic features (MMFs) → sunspot decay through diffusion

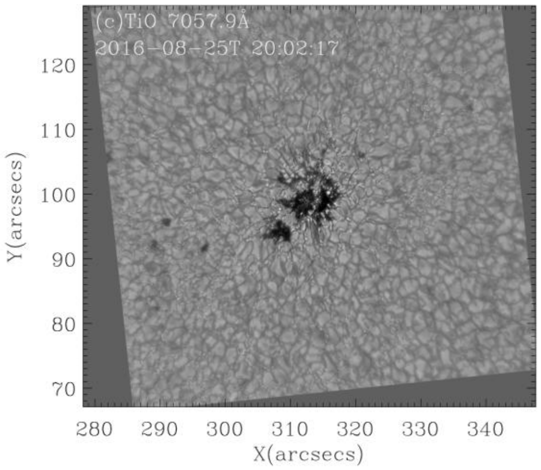

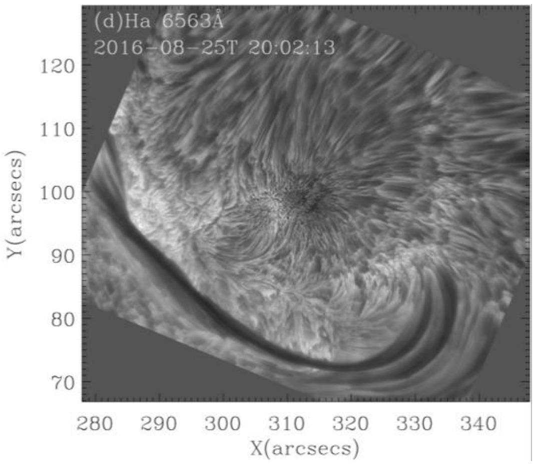

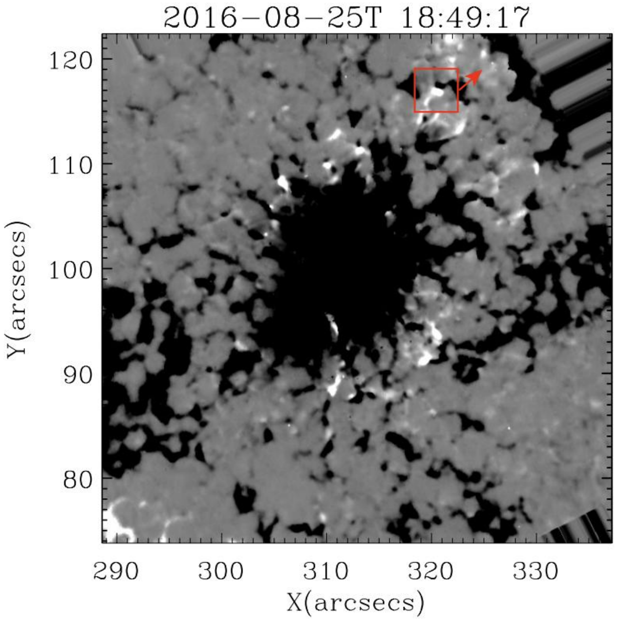

Zheng et al. 2024, A&A 686, A75

Supersonic Downflows in Active Regions

- GREGOR Infrared Spectrograph (GRIS) → He I λ1083.0 nm (HeLIx⁺) lines
- Supersonic downflows (0.2–6.4% area fraction) more prominent in the emerging phase → rising magnetic loops

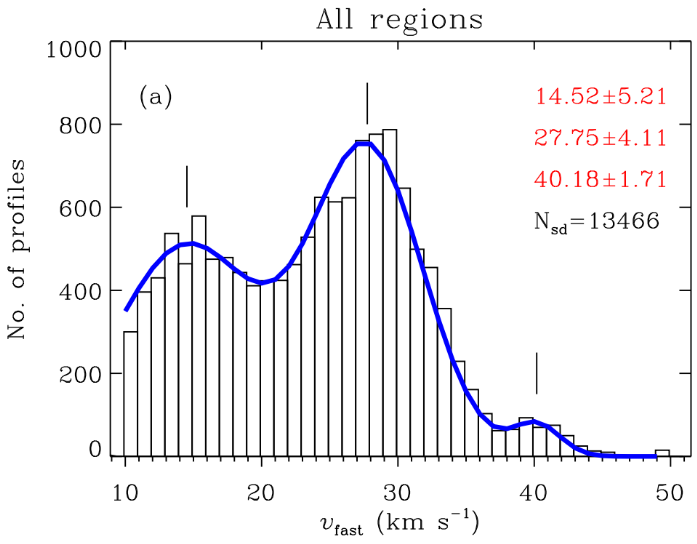

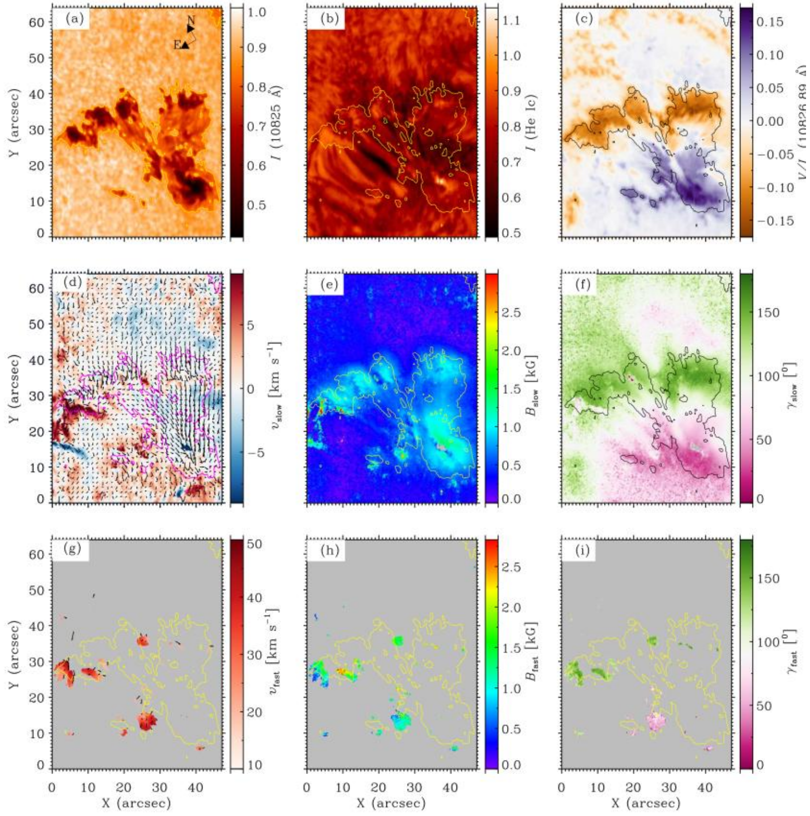

Sowmya et al. 2022, A&A 661, A122

Sunspot Umbra

– GREGOR Fabry-Pérot Interferometer (GFPI) → Fe I λ543.5 nm line and GREGOR Infrared Spectrograph (GRIS) → Si I λ1082.7 nm, Ca I λ1083.9 nm, He I λ1083.0 nm lines

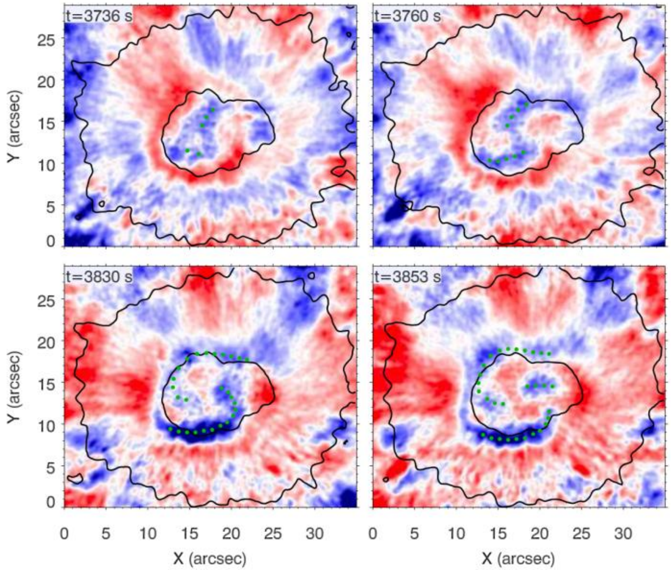

Felipe et al. 2018, A&A 621, A43

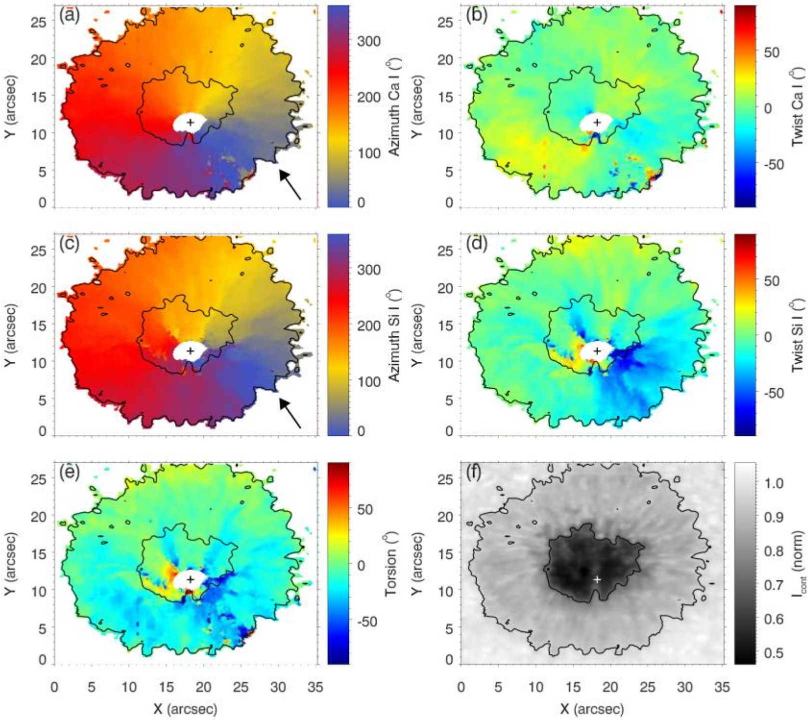

– Wave modes determined by thermal and magnetic sunspot structure

– Two-armed spiral wavefronts, outward propagating running penumbral waves → slow magnetoacoustic waves

Umbral Flashes

- DKIST Visible Spectro-Polarimeter (ViSP) → Fe I λ630.2 nm, Ca II H λ396.8 nm, and Ca II λ854.2 nm
- oscillatory “ridge” structures → intensity, central wavelength, line width, and linear and circular polarization
- Chromospheric 3-minute umbral oscillations
- Mach numbers (≈2) and speed (≈9 km s^{-1}) → magnetic field ($\Delta B \approx 50$ G), gas pressure, and temperature ($\Delta T / T \approx 0.1$)

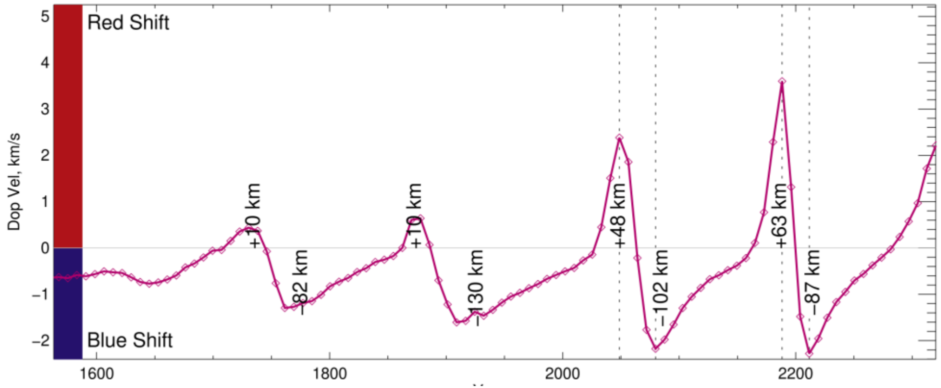

French et al. 2023, ApJ 945, L27

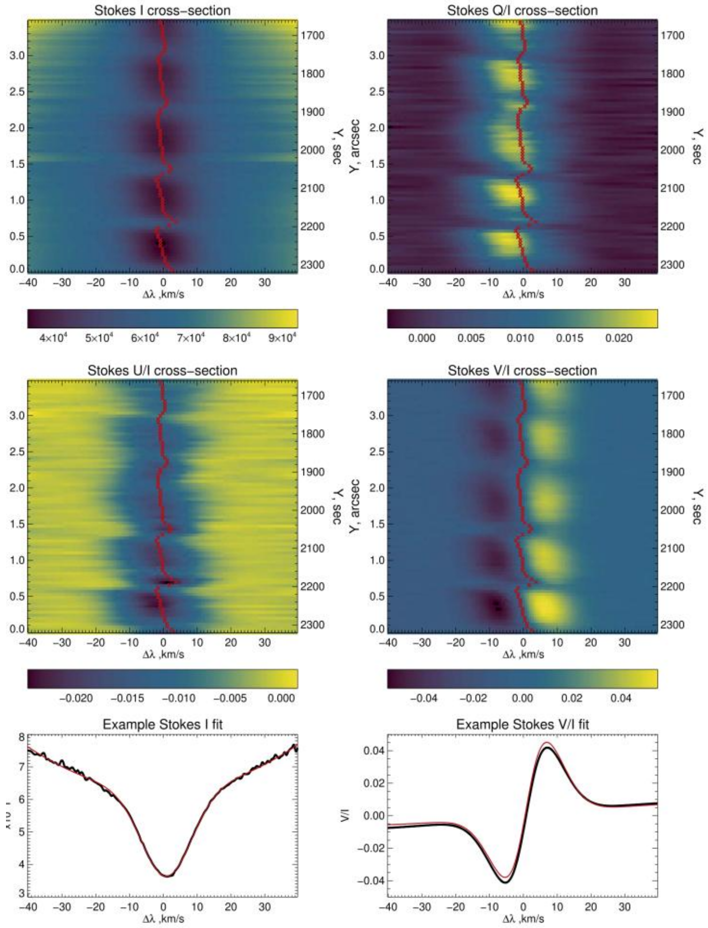

DKIST

Upper Chromospheric Magnetic Field of a Sunspot Penumbra

- GREGOR Infrared Spectrograph (GRIS) → Si I λ1082.7 nm and Ca I λ1083.9 nm (SPINOR) and He I λ1083.0 nm (HeLIx$^+$) lines
- Chromospheric variations coincide with variations in the inclination of the photospheric field → spine and interspine magnetic field structure
- log τ = 0.0, −0.7, −-2.3 and HeLIx+ (left to right)

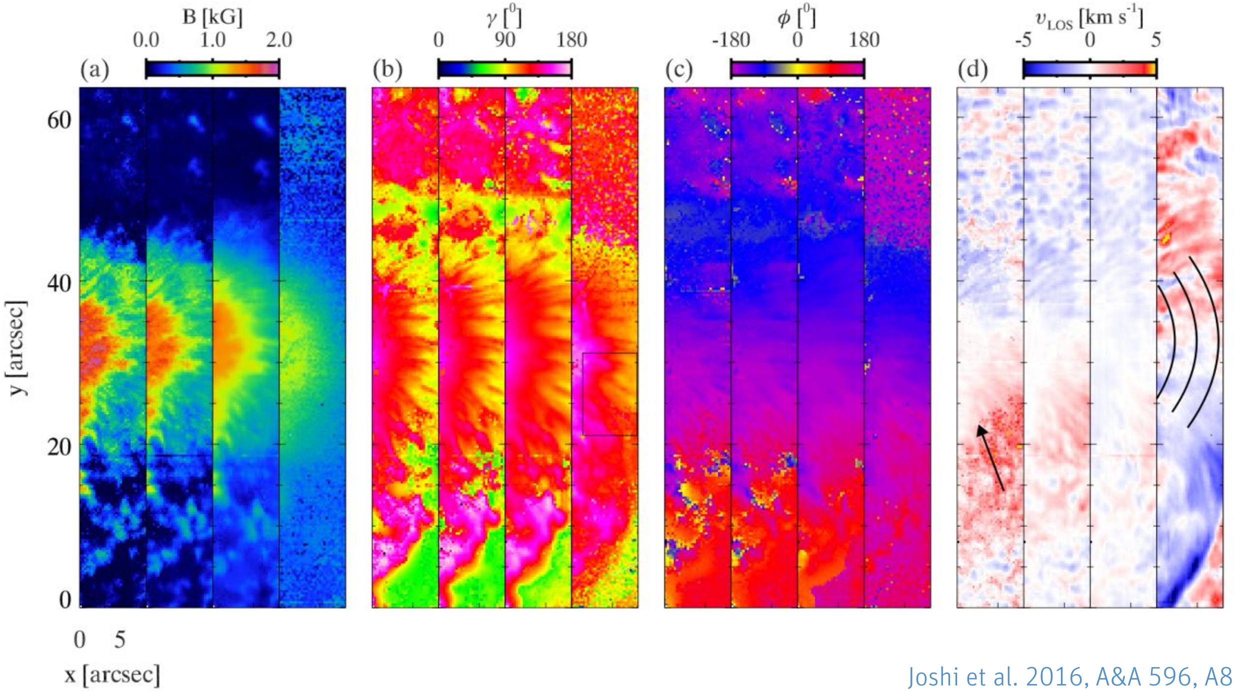

Joshi et al. 2016, A&A 596, A8

Light Bridges

Pores with Light Bridges

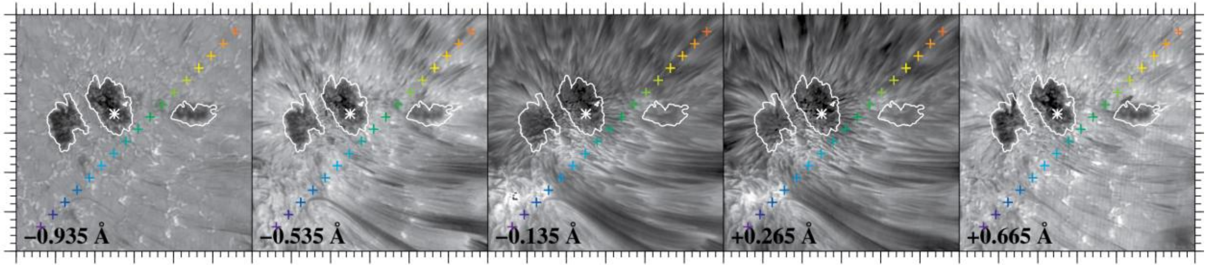

- GST Broadband Filter Imager (BFI) → TiO λ706 nm
- GST Visible Imaging Spectrometer (VIS) → Hα imaging spectroscopy
- Helioseismic and Magnetic Imager (HMI) → LOS magnetic field
- Pores show photospheric inflows while light bridges show outflows
- Strong radial chromospheric outflows at superpenumbral scales
- Border of pores and light bridges show strong variations
- Flux system connected to the surrounding supergranular cell

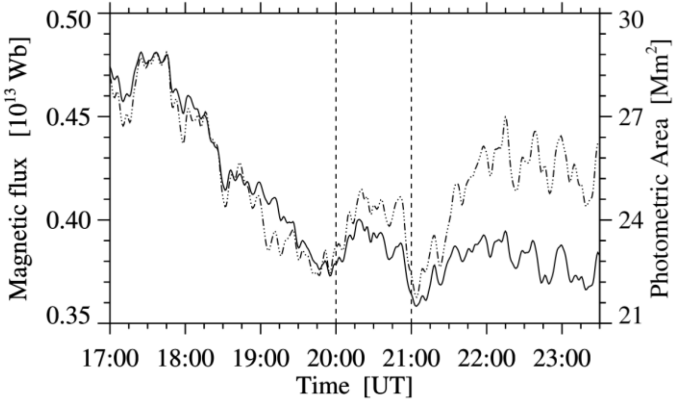

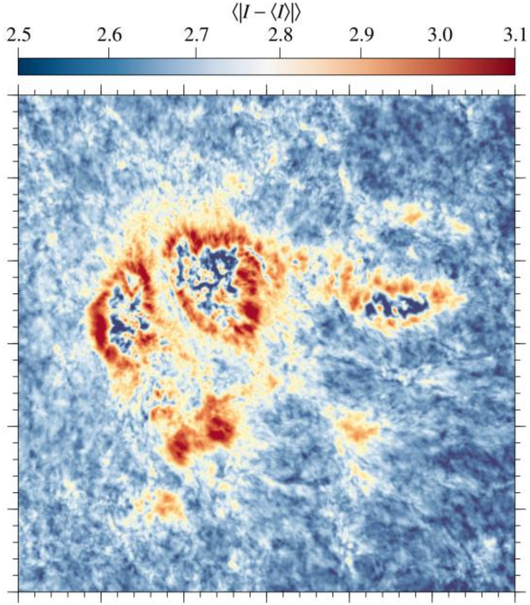

Kamlah et al. 2023, A&A 675, A182

Sunspot Light Bridge

- GREGOR Infrared Spectrograph (GRIS) → Si I λ1082.7 nm and Ca I λ1083.9 nm lines
- Light bridges are linked to sunspot decay → canopy with lower magnetic field strength in the inner part → convective flows → flow bend magnetic field lines and produces field reversals → strong vertical field lines

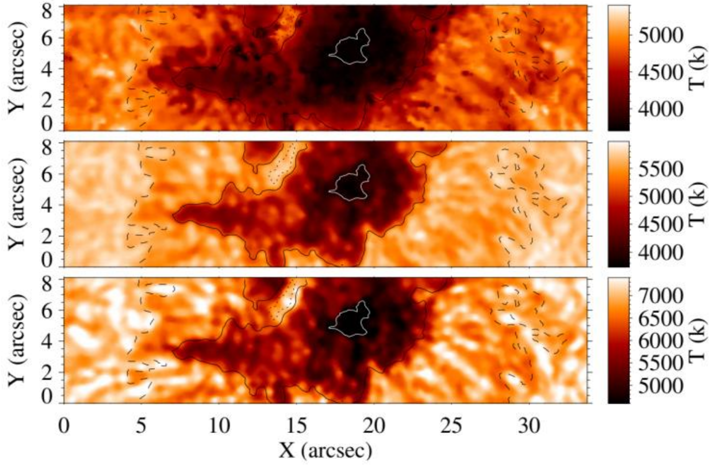

log τ = −2.2

log τ = −0.5

log τ = +0.3

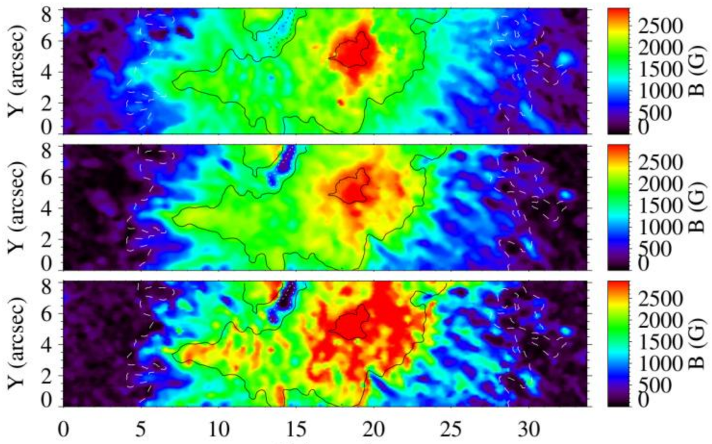

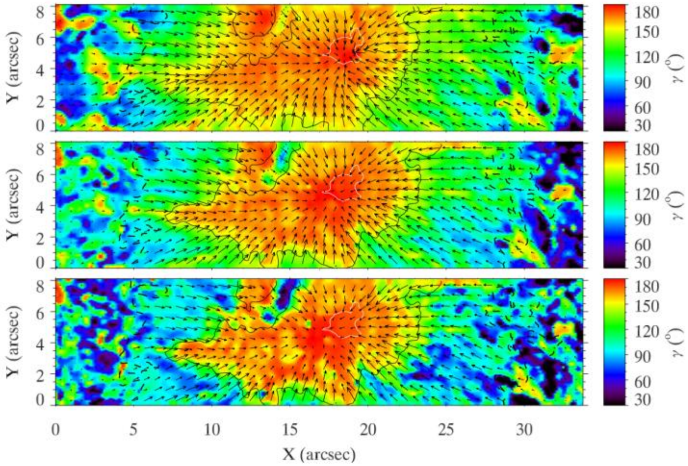

Felipe et al. 2016, A&A 596, 59

Disappearing Light Bridge and Penumbral Decay

- GREGOR Infrared Spectrograph (GRIS)
  → Si I λ1082.7 nm and Ca I λ1083.9 nm lines (SIR)
- GREGOR Fabry-Pérot Interferometer (GFPI)
  → Fe I λ617.3 nm line
- High-resolution Fast Imager (HiFI) → G-band and Ca II H

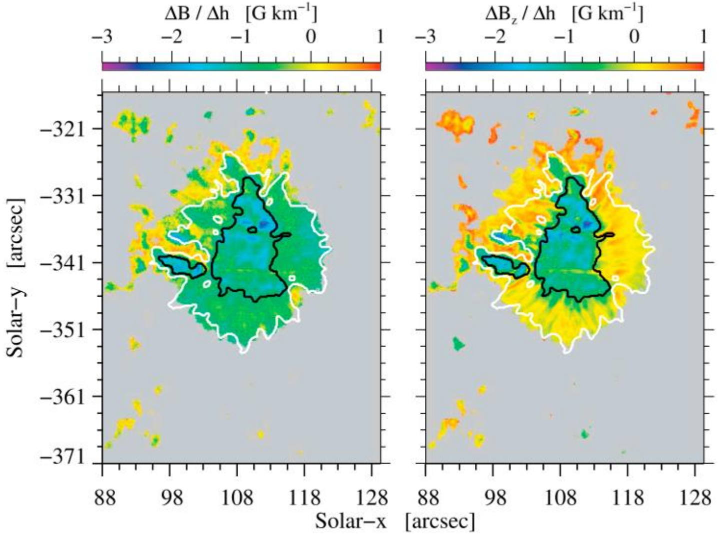

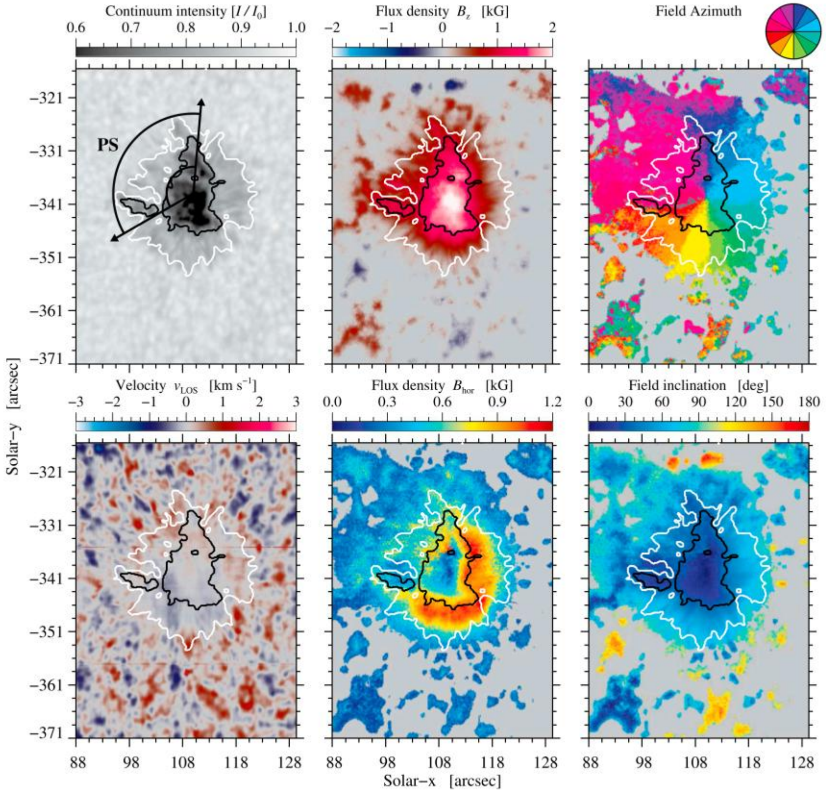

Verma et al. 2018, A&A 614, A2

Penumbra and Light Bridges

– Improved High-resolution Fast Imager (HiFI+) and GREGOR Infrared Spectrograph (GRIS) → Si I λ1082.7 nm (SIR) and He I λ1083.0 nm lines

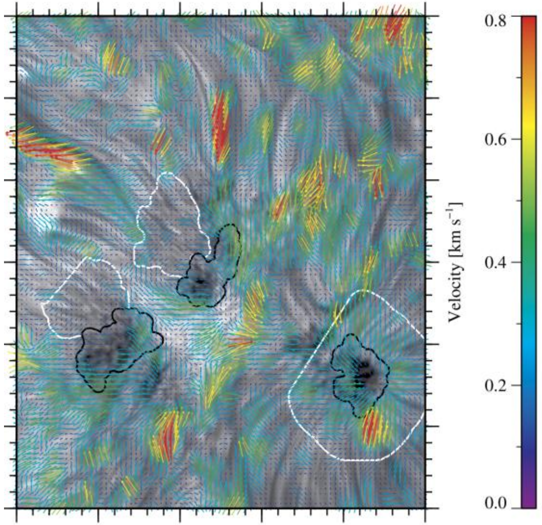

Kamlah et al. 2024, Sol. Phys. 299, 144

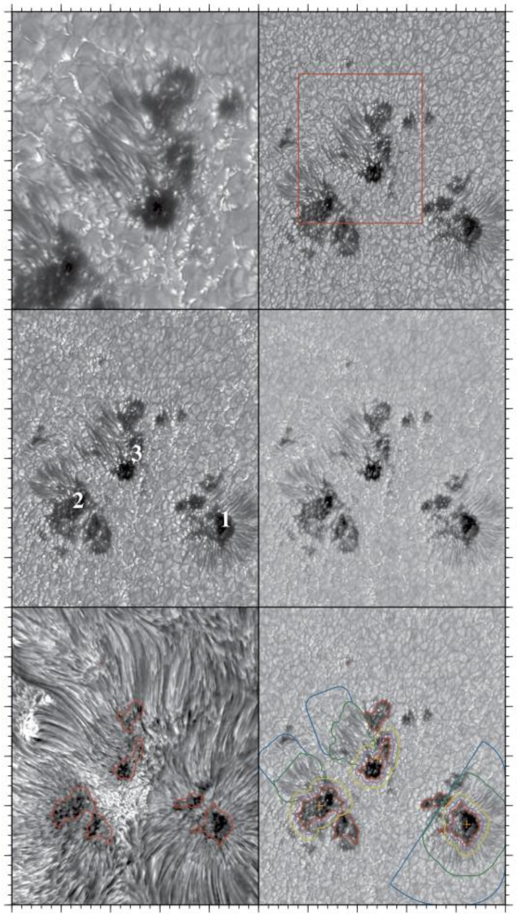

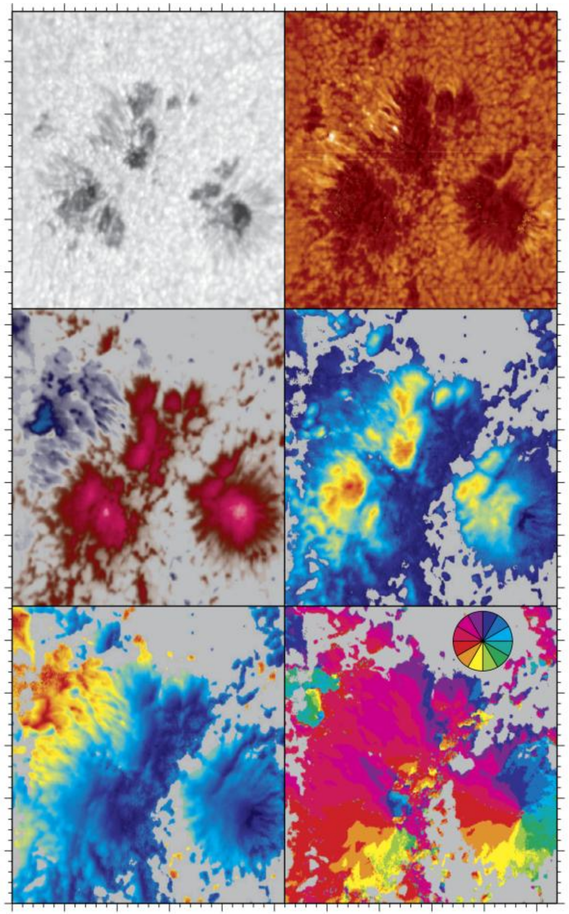

GREGOR

Flares

Flare-ejected Plasma Impacts on a Sunspot Light Bridge

- GREGOR Fabry-Pérot Interferometer (GFPI) → Fe I λ617.3 nm line
- High-resolution Fast Imager (HiFI) → G-band and Ca II H
- GREGOR Infrared Spectrograph (GRIS) → Fe I λ1565.5 nm lines
- C-class flare → photospheric and chromospheric brightenings, heating events, and Stokes-profiles
- Reconnection moves plasma blob along field lines interacting impacting a light bridge.

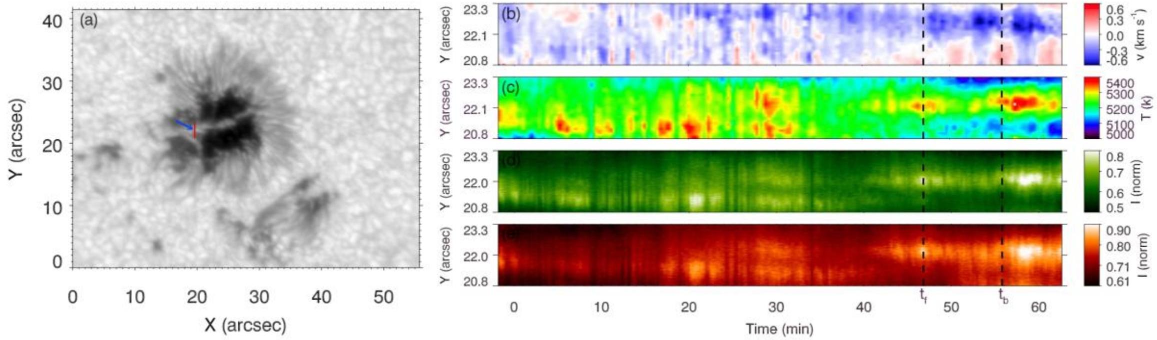

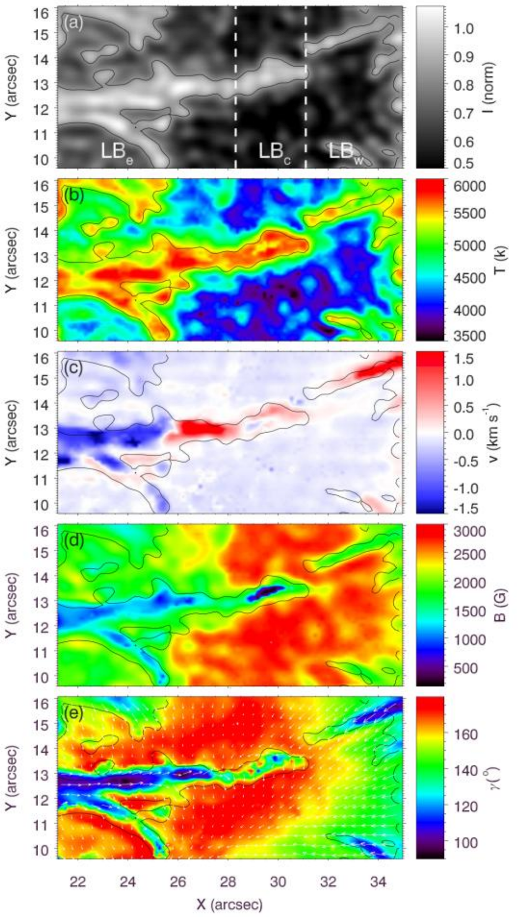

Felipe et al. 2017, A&A 608, A97

Recurring Flares

- GST Broadband Filter Imager (BFI) → TiO λ706 nm
- GST Visible Imaging Spectrometer (VIS) → Hα imaging spectroscopy
- Helioseismic and Magnetic Imager (HMI) → LOS magnetic field
- Atmospheric Imaging Assembly (AIA) → UV/EUV images
- Four confined flares followed by an eruptive flare, all associated with a jet with a twisted structure at flare peak
- Continuous injection of magnetic twist before and during the series of flares

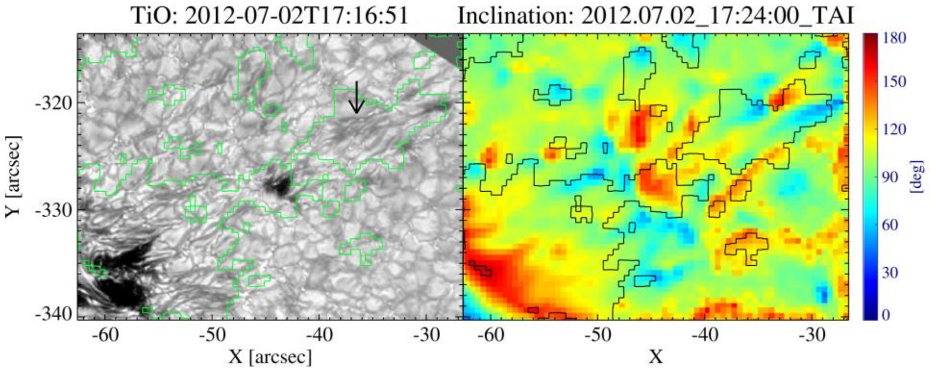

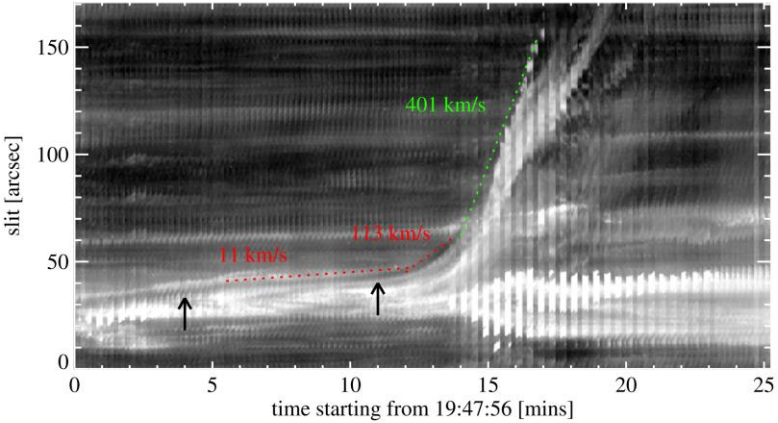

Lim et al. 2016, ApJ 817, 39

Pore Rotation and C-class Flare

- DKIST Visible Spectro-Polarimeter (ViSP)
  → G-band λ430.5 nm and Hβ λ486.1 nm
- DKIST Visible Spectro-Polarimeter (ViSP)
  → Fe I λ630.2 nm (ME-SPIN),
  Na I D_1 λ589.6 nm, and Ca II λ854.2 nm
- Helioseismic and Magnetic Imager (HMI)
  → LOS magnetic field
- Atmospheric Imaging Assembly (AIA)
  → UV/EUV images
- C4.1-class solar flare
- Complex magnetic field topology above rotating pores, null-point-like configuration
- 30% relative change in the horizontal component (δF_h) of Lorentz force at the flare peak time, no change in the radial component

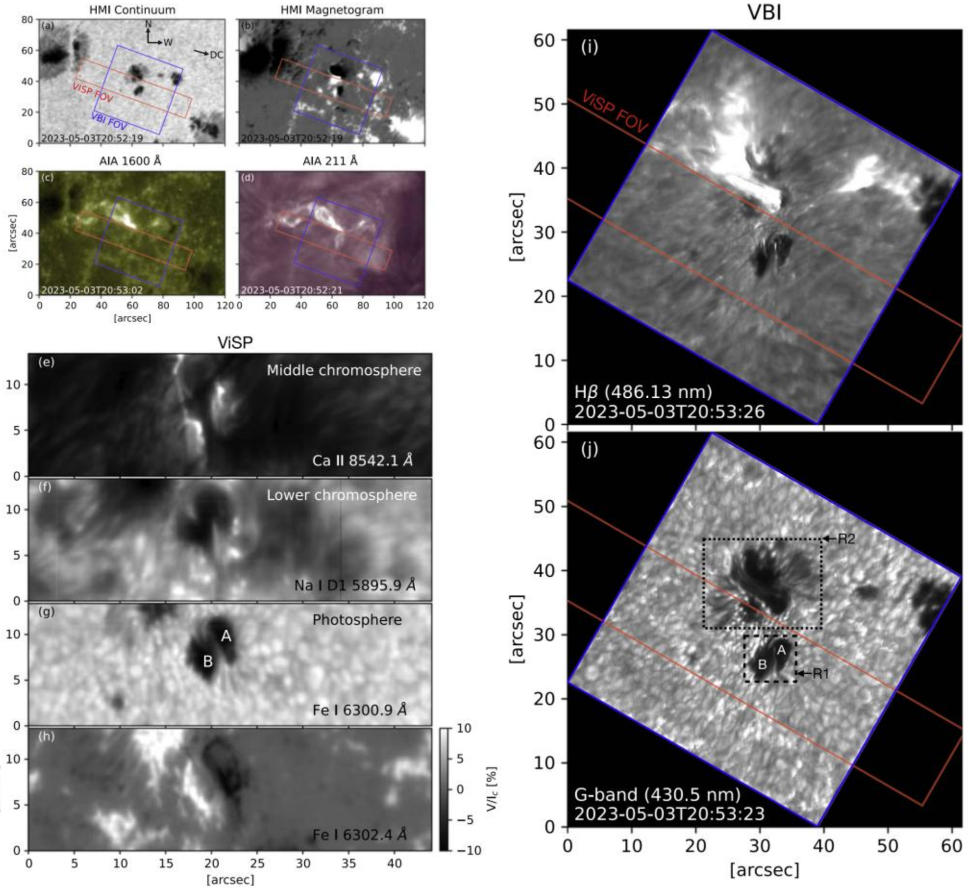

Yadav et al. 2024, ApJ 973, L10

Filaments

Arch Filament System

- GREGOR Infrared Spectrograph (GRIS) → He I λ1083.0 nm and Ca I λ1083.9 nm (SIR) lines
- Fibrils connects opposite polarities, i.e., the sunspot with small-scale fields near the polarity inversion line
- Moderate photospheric downflows are accompanied with stronger chromospheric downflows of about 10 km s^{-1}
- Rising flux tubes lift plasma into the chromosphere, where it cools and drains along the filament to the footpoints

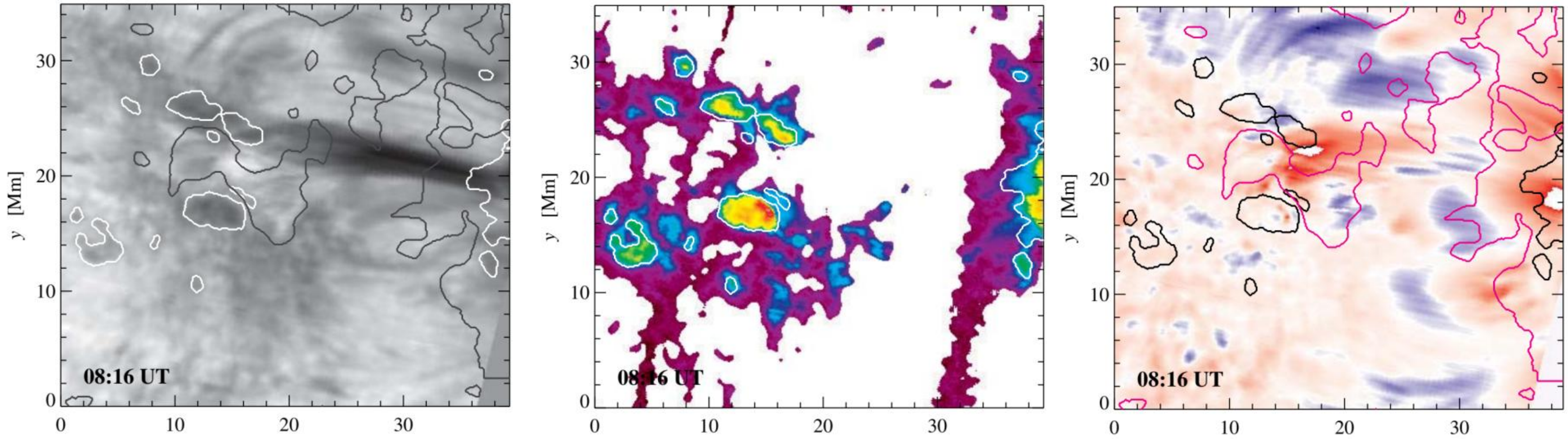

Balthasar et al. 2016, Astron. Nachr. 337, 1050

Emerging Flux Region and Arch Filament System

- GREGOR Infrared Spectrograph (GRIS) → Si I λ1082.7 nm (ME-SPIN) and He I λ1083.0 nm (HAZEL) lines
- Complex photospheric magnetic structure and smooth variation of chromspheric magnetic field (height ~2 Mm)
- NFF field extrapolation → loop height 10 Mm, loop with 20 Mm

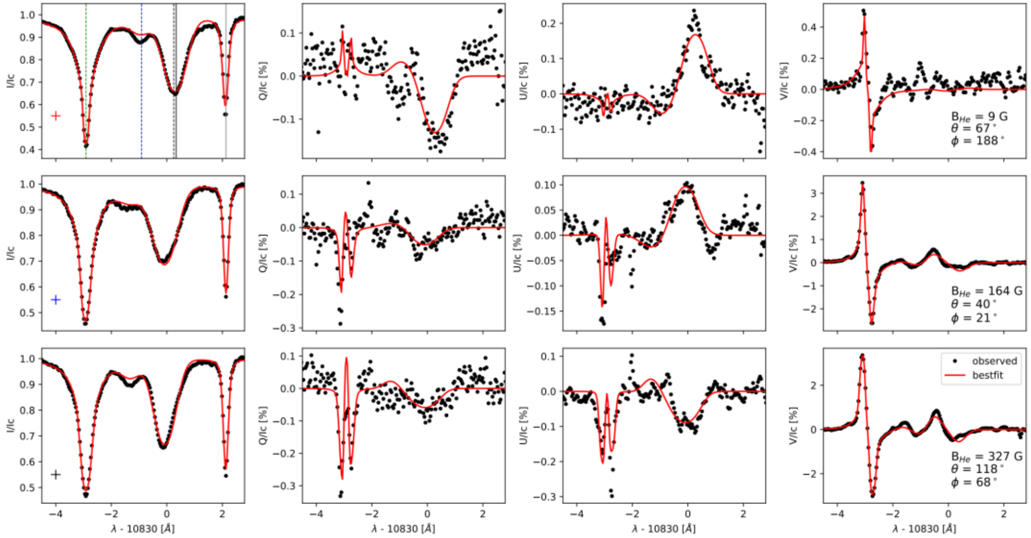

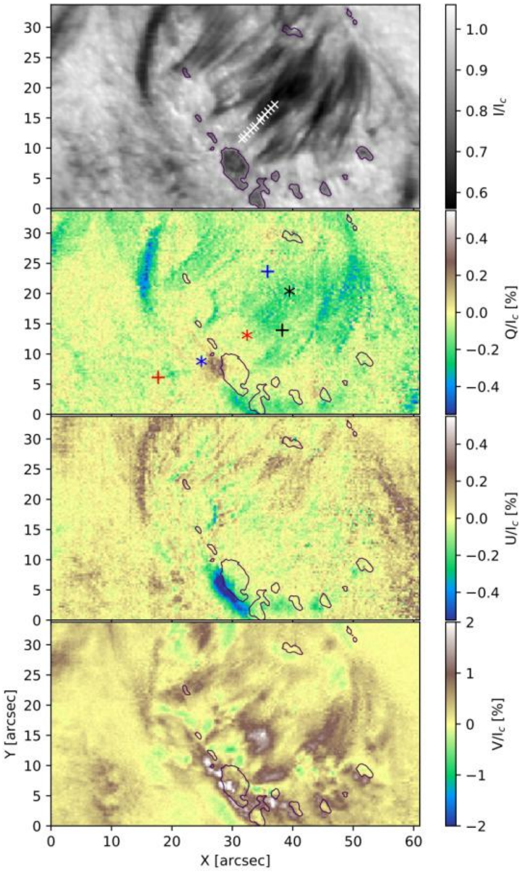

Yadav et al. 2019, A&A 632, A112

Active Region Filament

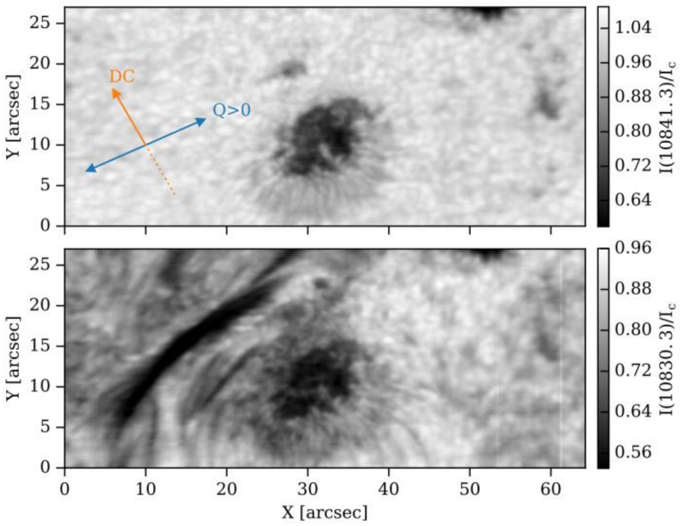

- GREGOR Infrared Spectrograph (GRIS) → Si I λ1082.7 nm (SIR) and He I λ1083.0 nm (HAZEL) lines
- More complex inversions are needed: absence of the filament in the He I Stokes-V map and difficulties in separating active region and filament fields

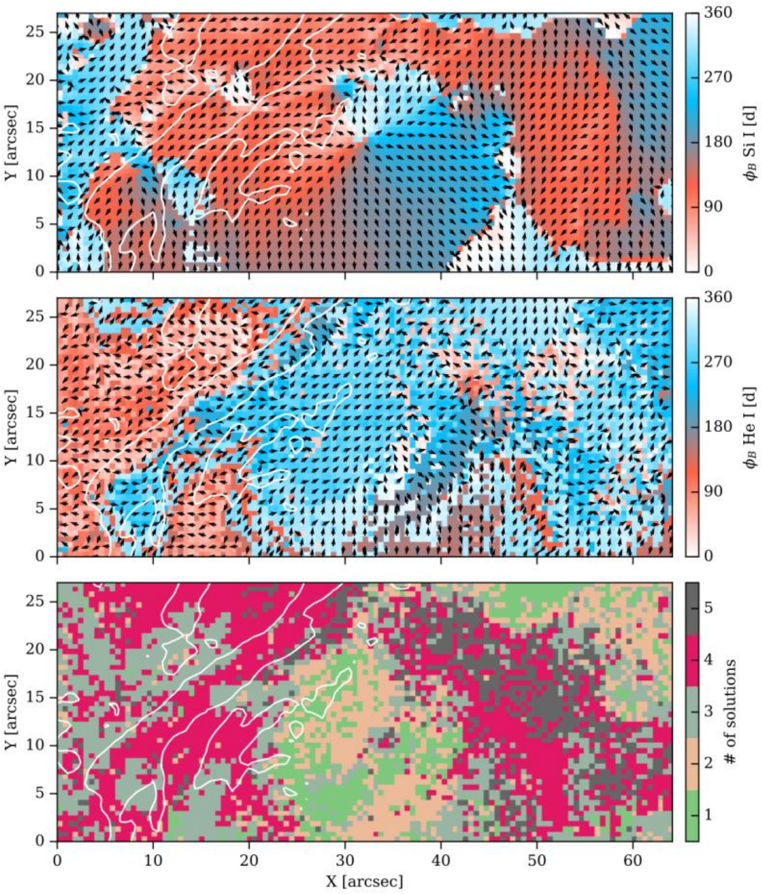

Díaz Baso et al. 2019, A&A 625, 128

Active Region Filaments and Jets

- GST Visible Imaging Spectrometer (VIS)
  → Hα imaging spectroscopy
- GST Broadband Filter Imager (BFI)
  → TiO λ706 nm
- Helioseismic and Magnetic Imager (HMI)
  → LOS magnetic field
- Atmospheric Imaging Assembly (AIA)
  → UV/EUV images
- Hinode Solar Optical Telescope (SOT)
  → LOS magnetograms and Dopplergrams
- Two-day observation of filament formation
- Cool material ($T \sim 10^4$ K) is ejected by a series of jets
- Magnetic reconnection between pre-existing and newly emerging magnetic fields

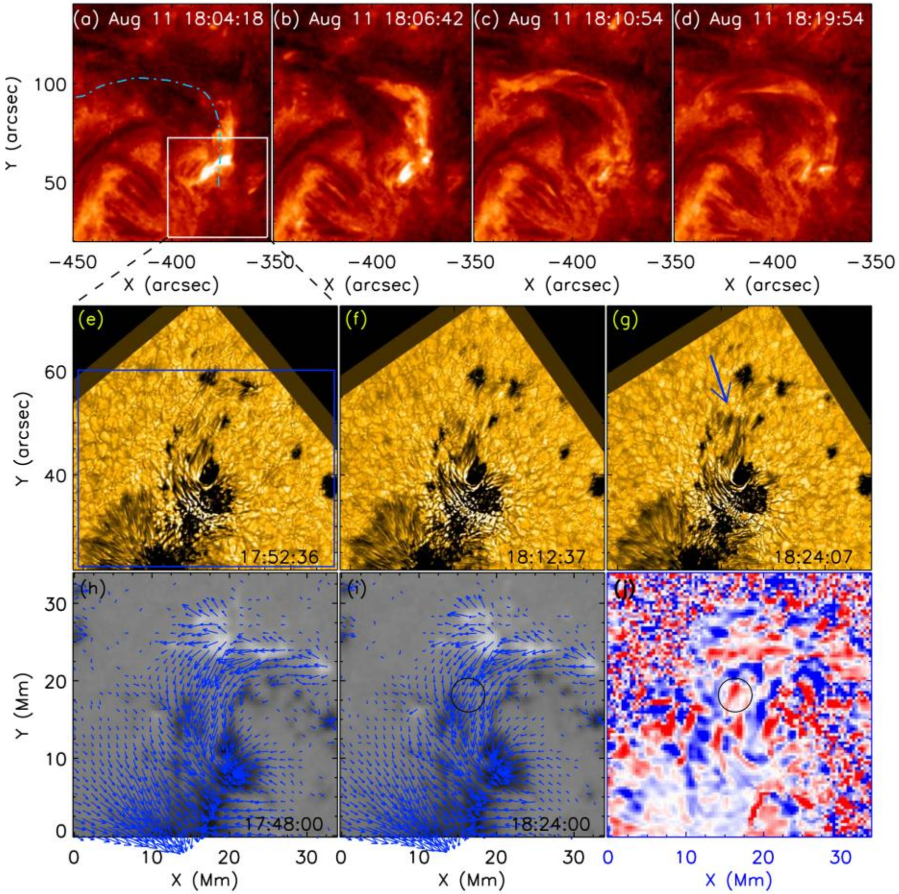

Wang et al. 2018, ApJ 863, 180

BBSO

Quiet Sun

Quiet Sun Magnetism

- DKIST Visible Spectro-Polarimeter (ViSP) $\rightarrow$ Fe I λ630.2 nm (SIR)
- Search for the best multi-inversion strategy by means of MHD simulations (MANCHA3D)
- Fe I lines at 1.5 μm offer better diagnostics for quiet-Sun magnetic field observations
- Multiline inversions $\rightarrow$ broad range of excitation potentials, log (gf) values, and effective Landé factors g_{eff} $\rightarrow$ diversity improves capacity to accurately retrieve atmospheric structure and magnetic properties

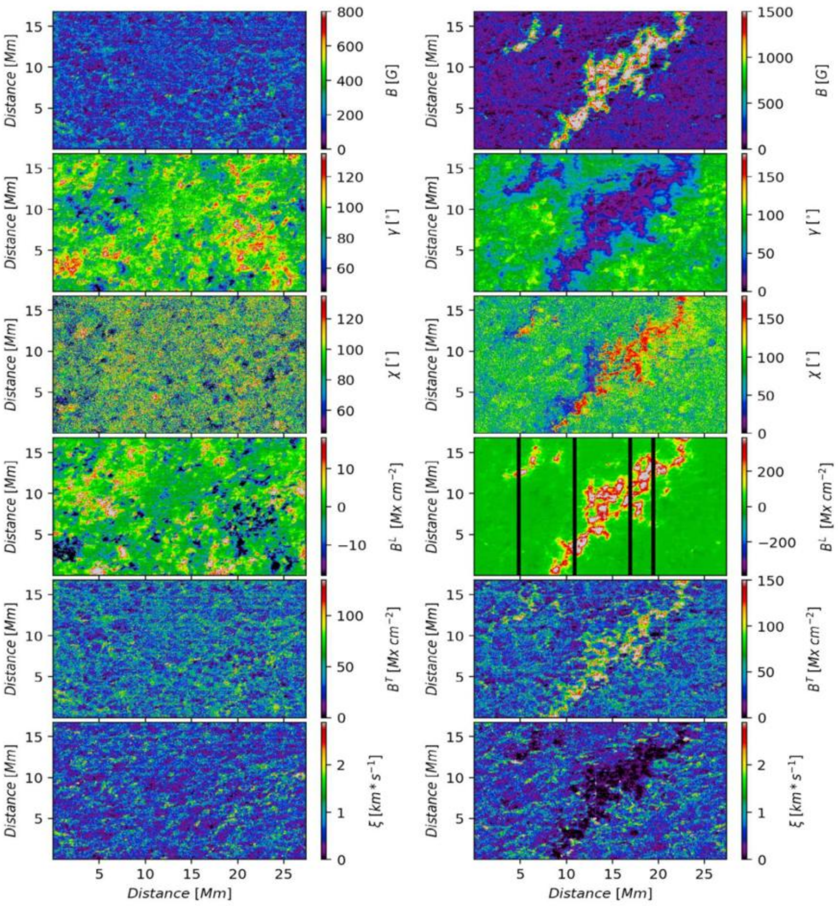

Trelles Arjona 2025, ApJ 986, 169

Striated Granular Edges

- DKIST Visible Spectro-Polarimeter (ViSP) → G-band
- Proxy magnetometry
- Multidimensional Radiative MHD (MURaM) simulation
- Striation structure widths of 20–50 km
  → spatial variations in photospheric magnetic flux concentrations

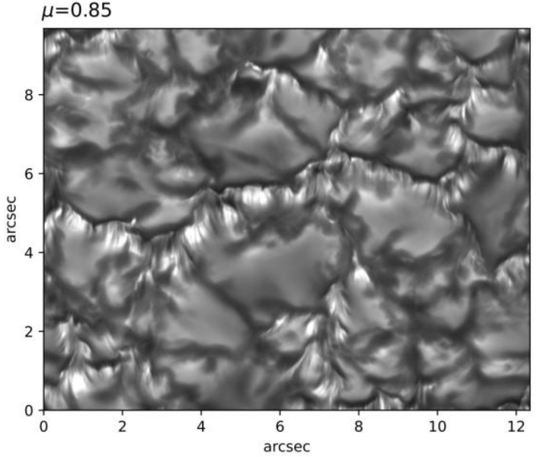

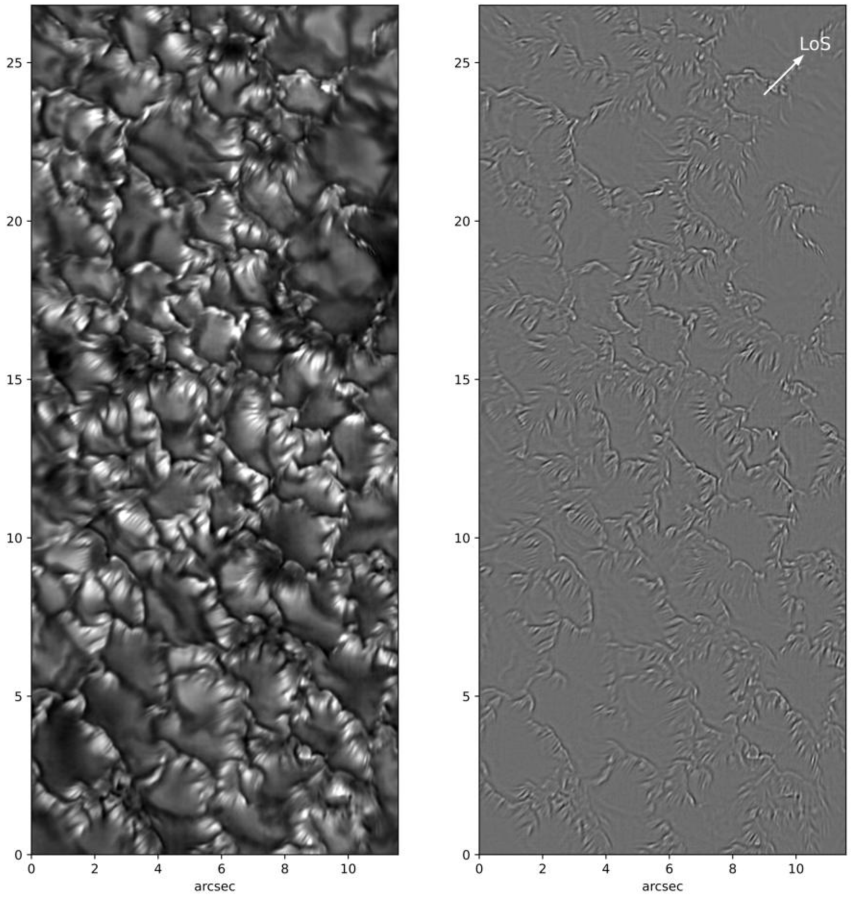

Kuridze et al. 2023, ApJ 985, L23

Chromospheric Solar Plage

- DKIST Visible Broadband Imager (VBI) → Hβ λ486.1 nm
- DKIST Visible Spectro-Polarimeter (ViSP) → Fe I λ630.2 nm and Ca II λ854.2 nm
- Inversion indicate dense fibrils in the Ca II λ 854.2 nm line → overdense fibrils responsible for spectral line broadening of chromospheric fine-scale structures

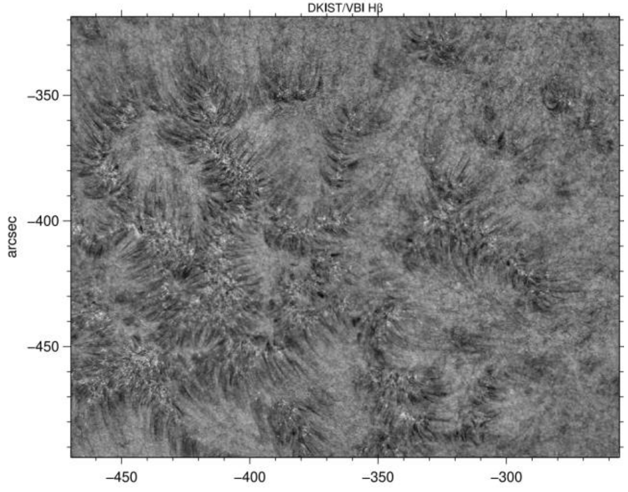

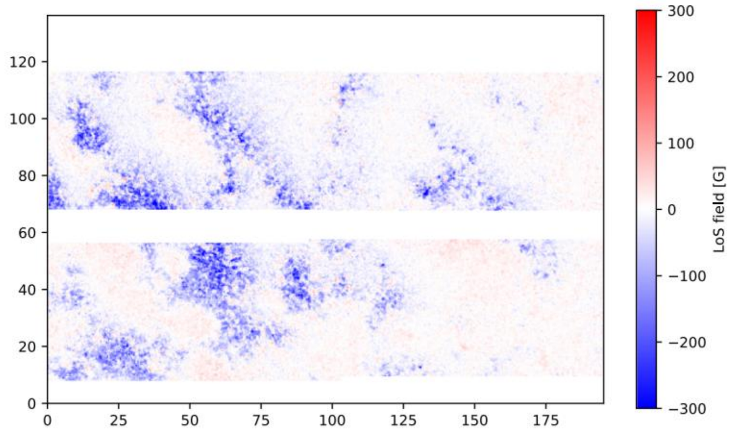

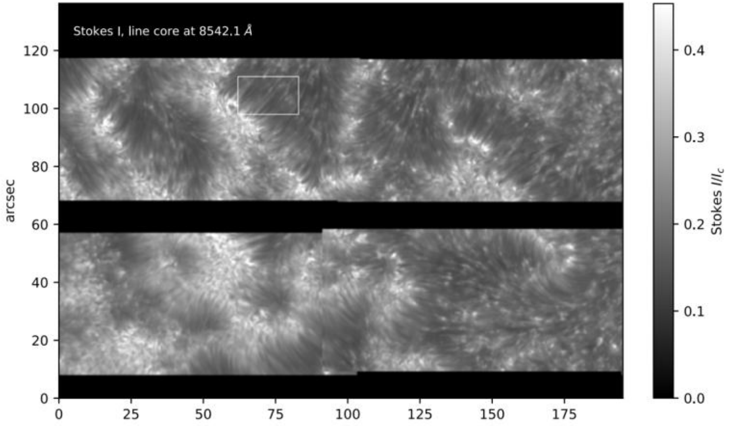

Kuridze et al. 2024, ApJ 965, 15

DKIST

Spicules and Microfilament Eruptions

- GST Visible Imaging Spectrometer (VIS) → Hα imaging spectroscopy
- GST Near Infra- Red Imaging Spectro-polarimeter (NIRIS) → LOS magnetic field
- Hinode Solar Optical Telescope (SOT) → Ca II H
- Hinode EUC Imaging Spectrometer (EIS) → He II λ25.6 nm
- Erupting microfilaments might drive enhanced spicular activity → twisting-type motions of 20–50 km s^{-1} in the associated jet and 20–30 km s^{-1} in enhanced specular activity
- Erupting microfilaments are analogues to minifilament eruptions, which are fundamental driver of coronal jets

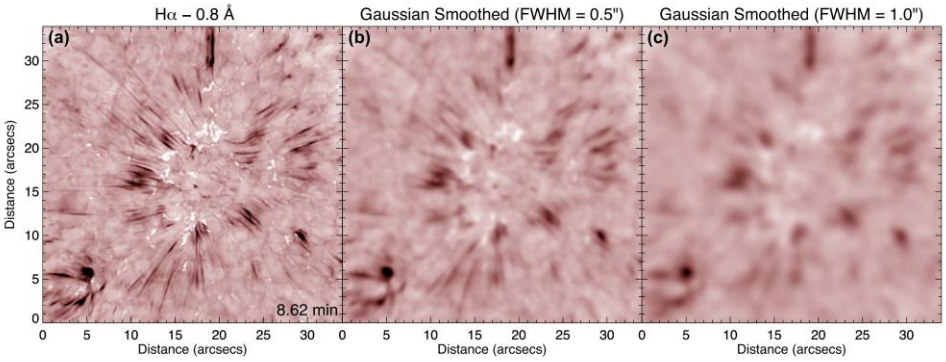

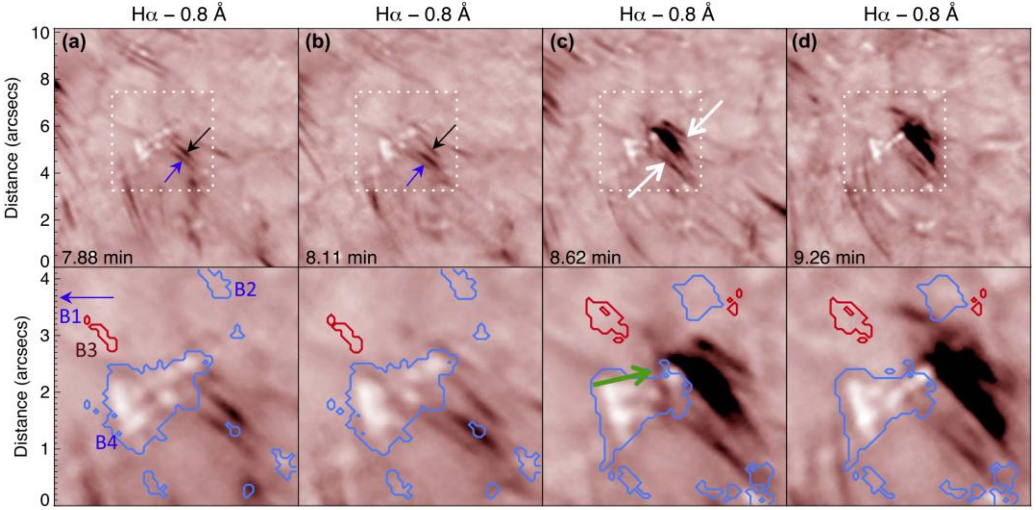

Sterling et al. 2020, ApJ 893, L45

Origin of Type II Spicules

- GST Near Infra- Red Imaging Spectro-polarimeter (NIRIS) → LOS magnetic field
- GST Visible Imaging Spectrometer (VIS) → Hα imaging spectroscopy
- GST Broadband Filter Imager (BFI) → TiO λ706 nm
- Statistical study of quiet-Sun areas → extrapolate a series of potential field configurations and study their time variations
- Areas with (footpoints of Hα features) and without changes in loop connectivity
- Separatrix between open- and closed-loop systems → rapid blue- and red-shifted excursions (type II spicules)

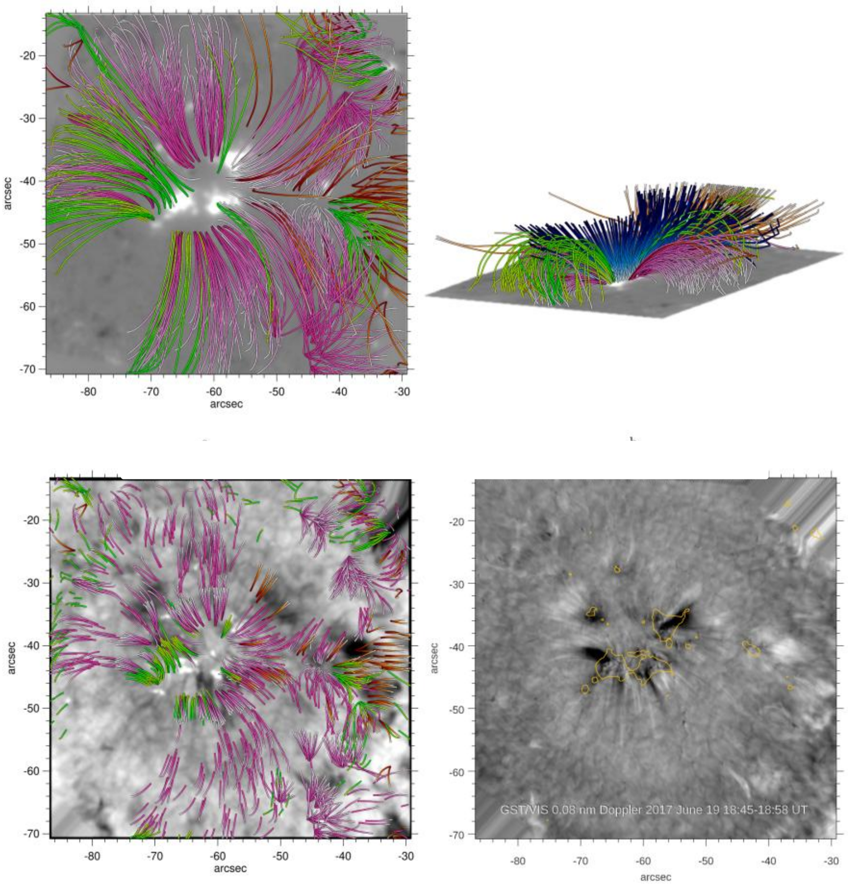

Yurchyshyn et al 2024, ApJ 961, 79

Summary

- Many new observations with high spatial, temporal, and spectral resolution and high polarimetric accuracy
- Multi-wavelength and multi-instrument observations are the key ingredients to scientific discovery
- Synergies between space missions and ground-based observations
- Field-of-view, even with mosaics, still limited
  → telescopes are still needed that bridge the gap between high-resolution and synoptic observations
- A meta-study of high-resolution observations during the last 15 years is missing.

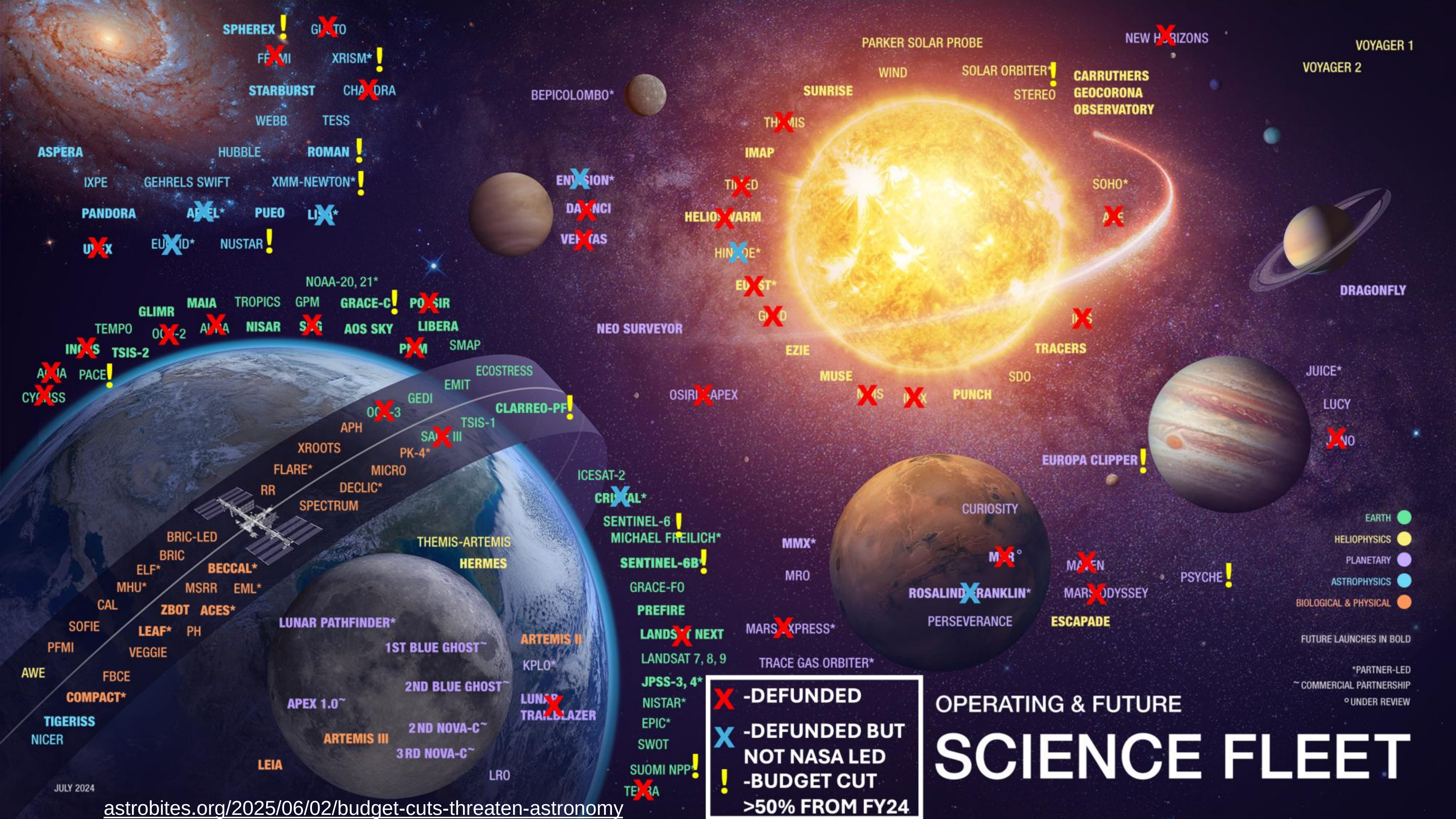

SPHEREX
GI TO
F MI
XRISM*
STARBURST
CHA DRA
WEBB
TESS
ASPERA
HUBBLE
ROMAN
IXPE
GEHRELS SWIFT
XMM-NEWTON*
PANDORA
A EL*
PUEO
LI A*
U EX
EU ID*
NUSTAR
BEPICOLOMBO*
EN SION*
DA NCI
VE TAS
PARKER SOLAR PROBE
WIND
SOLAR ORBITER*
STEREO
SUNRISE
CARRUTHERS
GEOCORONA
OBSERVATORY
NEW H RIZONS
VOYAGER 1
VOYAGER 2
TH MIS
IMAP
TI ED
HELIO WARM
HIN DE*
EU ST*
G LD
SOHO*
A S
DRAGONFLY
NEO SURVEYOR
EZIE
MUSE
I S
TRACERS
SDO
OSIRI APEX
M S
I X
PUNCH
JUICE*
LUCY
J NO
EUROPA CLIPPER
NOAA-20, 21*
GLIMR
MAIA
TROPICS
GPM
GRACE-C
PO SIR
TEMPO
OC -2
A A
NISAR
S G
AOS SKY
LIBERA
IN S
TSIS-2
P M
SMAP
A IA
PACE
CY ISS
ECOSTRESS
EMIT
GEDI
CLARREO-PF
OC -3
APH
TSIS-1
SA III
XROOTS
PK-4*
FLARE*
MICRO
RR
DECLIC*
SPECTRUM
ICESAT-2
CRI AL*
SENTINEL-6
MICHAEL FREILICH*
SENTINEL-6B*
GRACE-FO
PREFIRE
LANDS T NEXT
LANDSAT 7, 8, 9
JPSS-3, 4*
NISTAR*
EPIC*
SWOT
SUOMI NPP
TE RA
BRIC-LED
BRIC
ELF*
BECCAL*
MHU*
MSRR
EML*
CAL
ZBOT
ACES*
SOFIE
LEAF*
PH
PFMI
VEGGIE
AWE
FBCE
COMPACT*
TIGERISS
NICER
THEMIS-ARTEMIS
HERMES
LUNAR PATHFINDER*
1ST BLUE GHOST~
ARTEMIS II
KPLO*
2ND BLUE GHOST~
APEX 1.0~
LUNA
TRA BLAZER
2ND NOVA-C~
ARTEMIS III
3RD NOVA-C~
LEIA
LRO
MMX*
MRO
CURIOSITY
M R°
MA EN
PSYCHE
ROSALIND RANKLIN*
MARS ODYSSEY
PERSEVERANCE
ESCAPADE
MARS XPRESS*
TRACE GAS ORBITER*
EARTH
HELIOPHYSICS
PLANETARY
ASTROPHYSICS
BIOLOGICAL & PHYSICAL
FUTURE LAUNCHES IN BOLD
*PARTNER-LED
~ COMMERCIAL PARTNERSHIP
° UNDER REVIEW
OPERATING & FUTURE
SCIENCE FLEET
JULY 2024
X -DEFUNDED
X -DEFUNDED BUT NOT NASA LED
! -BUDGET CUT >50% FROM FY24
astrobites.org/2025/06/02/budget-cuts-threaten-astronomy